

A Comparative Study and Analysis on Techniques for Diffusion-Weighted Magnetic Resonance Imaging

Yuan-Hung Wu, Wen-Yi Issac Tseng, and Chein-I Chang, *Senior Member, IEEE*

Abstract—Neural scientists have long been eager to find the subcortical pathways between different parts of cortex in human brain. By far, Diffusion Weighted-Magnetic Resonance Imaging (DW-MRI) is the only noninvasive technique to achieve this task *in vivo*. It applies a bipolar gradient to reveal diffusion of water molecules. With the assumption that the directions of neural fibers parallel to the directions in which water molecules diffuse, we can use the DW-MRI to track the neural fibers. Various signal processing techniques have been developed in extracting the directional information via DW-MRI. In this study, four techniques that are currently being used but have not been rigorously compared for performance are evaluated via custom-designed synthetic data and phantoms. By combining different techniques in accordance with their specialties, a better approach to track finer subcortical pathways *in vivo* can be derived and used to verify theories in human brain mapping.

I. INTRODUCTION

THE ultimate task for researchers in the field of signal processing is to extract most useful information from the data corrupted by noise. In DW-MRI that is used to serve the purpose of neural fiber tractography, the information we care most is the direction(s) of neural fiber(s) in each voxel. Diffusion Tensor Imaging (DTI) [1] has been the first available model. It is fast and easy to implement since only linear least square method is required. Based on it, three dimensional tracking of white matter in human brain has been made [2]. Using Markov Chain-Monte Carlo (MCMC) method on DTI, the uncertainty of the fiber direction is retained [3], and the corresponding MCMC tracking algorithm was applied in tracking connection between thalamus and cortex [4]. However, DTI has the limitation that only one direction can be inferred from each voxel. In fiber crossings with more than one direction, it will obtain spurious results due to the nature of its model. Diffusion Spectrum Imaging (DSI) [5] is one way to resolve fiber crossings, but it requires more gradients, which means longer on-line time, than DTI. National Taiwan University Hospital has

conducted a series of experiments in assessing the accuracy of both DTI and DSI [6] [7]. Persistent Angular Structure (PAS) [8] is another way to extract more than one direction from each voxel in DW-MRI. Applying the maximum entropy principle in extracting the angular information, it is theoretically more robust than DSI in finding the correct fiber direction(s) in noise-corrupted NMR signal with the same number of gradients. However, no study has been conducted as we know in assessing the technique. Therefore, in this study, we would like first to use computer-generated synthetic data to compare DTI, DTI with directional uncertainty, DSI, and PAS. And then we would like to assess these four techniques on real MRI with known phantom.

The paper consists of 5 parts. After the introduction, we briefly describe each technique in part 2. In part 3, computer-generated synthetic data, phantom, and the comparing method are stated. Before drawing the conclusion, the experimental result is stated in part 4.

II. METHODS

A. Diffusion Tensor Imaging

DTI models the diffusion of water molecules in each voxel as an effective diffusion tensor \mathbf{D}^{eff} , which relates the macroscopic concentration gradient, ∇C , and macroscopic diffusive flux, \mathbf{J} , in an anisotropic medium:

$$\begin{bmatrix} J_x \\ J_y \\ J_z \end{bmatrix} = - \begin{bmatrix} D_{xx}^{\text{eff}} & D_{xy}^{\text{eff}} & D_{xz}^{\text{eff}} \\ D_{yx}^{\text{eff}} & D_{yy}^{\text{eff}} & D_{yz}^{\text{eff}} \\ D_{zx}^{\text{eff}} & D_{zy}^{\text{eff}} & D_{zz}^{\text{eff}} \end{bmatrix} \begin{bmatrix} \frac{\partial C}{\partial x} \\ \frac{\partial C}{\partial y} \\ \frac{\partial C}{\partial z} \end{bmatrix} \quad (1)$$

For uncharged moieties such as water, \mathbf{D}^{eff} is symmetric, i.e., $\mathbf{D}^{\text{eff}} = \mathbf{D}^{\text{eff}T}$. And we will denote \mathbf{D}^{eff} as \mathbf{D} thereafter for simplicity. The NMR signal measurement is related to \mathbf{D} as

$$A(\underline{q}) \equiv \frac{A^*(\underline{q})}{A^*(0)} = \exp(-t \underline{q}^T \underline{D} \underline{q}) \quad (2)$$

, where $A(\underline{q})$ is the NMR signal attenuation, and $\underline{q} = \gamma \underline{g} \Delta$, γ being the gyromagnetic ratio, a constant, and \underline{g} being the magnetic gradient. We may acquire each element of \mathbf{D} by least square method. And the neural fiber direction is deduced by parallel to the eigenvector of \mathbf{D} with largest eigenvalue.

Manuscript received on April 8, 2005.

Yuan-Hung Wu is with the Department of Computer Science and Electrical Engineering, University of Maryland, Baltimore County, Baltimore, MD 21250, USA (phone: 410-455-6583; e-mail: ywu1@umbc.edu)

Wen-Yi Issac Tseng is with Department of Radiology, National Taiwan University Hospital, Taipei, Taiwan, Republic of China

Chein-I Chang is with the Department of Computer Science and Electrical Engineering, University of Maryland, Baltimore County, Baltimore, MD 21250, USA

B. DTI with Directional Uncertainty

Instead of fitting a deterministic \mathbf{D} with measurements, we may also introduce random variables into the model to be fitted. With the help of MCMC algorithm, we may obtain the *pdf* of directional angle of the fiber.

C. Persistent Angular Structure

The ensemble averaged diffusion of water molecules within a voxel is characterized by a 3-d *pdf* $p(\mathbf{x})$, \mathbf{x} being the displacement after time Δ . In DW-MRI, we can infer $p(\mathbf{x})$ from the following relation:

$$A(\underline{q}) = \int_{\mathbb{R}^3} p(\underline{x}) \exp(-i\underline{q} \cdot \underline{x}) d\underline{x} \quad (3)$$

, where $A(\underline{q})$ is the signal attenuation and $\underline{q} = \gamma \underline{g} \Delta$, γ being the gyromagnetic ratio, a constant, and \underline{g} being the magnetic gradient. Since the diffusion of water molecules has the symmetric property $p(\mathbf{x})=p(-\mathbf{x})$,

$$A(\underline{q}) = \int_{\mathbb{R}^3} p(\underline{x}) \cos(-\underline{q} \cdot \underline{x}) d\underline{x}$$

(4)

Usually only angular information of $p(\mathbf{x})$ is important to us. To simplify computation, we limit the *pdf* inferred from data to be

$$p(\underline{x}) = \tilde{p}(\hat{x}) \delta(|\underline{x}| - r)$$

(5)

, and $\hat{x} \equiv \frac{\underline{x}}{|\underline{x}|}$, the unit vector of \mathbf{x} . That is, $p(\mathbf{x})$ can only have

nonzero value $\tilde{p}(\hat{x})$ on the surface of a sphere with radius r . From the maximum entropy distribution theory, we know $\tilde{p}(\hat{x})$ must be of the form

$$\tilde{p}(\hat{x}) = \exp\left(\lambda_0 + \sum_{i=1}^M \lambda_i \exp(-i\underline{q}_j \cdot r\hat{x})\right) \quad (6)$$

to have the maximal entropy. Applying the property $p(\mathbf{x})=p(-\mathbf{x})$ here, we have

$$\tilde{p}(\hat{x}) = \exp\left(\lambda_0 + \sum_{i=1}^M \lambda_i \cos(\underline{q}_j \cdot r\hat{x})\right) \quad (7)$$

Now, our task has become selecting a proper r and fitting $(\lambda_0, \lambda_1, \dots, \lambda_N)$ to the observed data. By searching for local maxima of $\tilde{p}(\hat{x})$, we find principle directions of fibers.

D. Diffusion Spectrum Imaging

DSI assumes the same Fourier pair between the NMR signal attenuation and the diffusion *pdf* of water molecules as in PAS. But it applies a set of 515 different gradients to each voxel to acquire the *pdf* by inverse FFT. And to infer the principle directions, it defines fiber Orientation Distribution Function(ODF) as

$$\psi(\underline{u}) = \int_0^{r_{\max}} P_s(r\underline{u}) r^2 dr \quad (8)$$

, where P_s is the *pdf* derived by iFFT, and \underline{u} is the unit vector. By searching the local maxima of ODF, the principle directions are determined.

III. EXPERIMENT

A. The Synthetic Data

We test the algorithms on a range of simple test functions for $p(\mathbf{x})$. We use the simple diffusion model together with the statistical results of Pierpaoli *et al* [9] to simulate measurements from the brain. To simulate measurements from dense-white-matter regions we use the diffusion tensor $10^{-10} \text{diag}(17, 2, 2) \text{m}^2 \text{s}^{-1}$, where $\text{diag}(X, Y, Z)$ is the diagonal matrix with leading diagonal elements $X, Y,$ and Z . On average, the apparent diffusion tensor in grey matter is closer to isotropic than in white matter, but of the same order of magnitude [9]. We simulate measurements from white-matter fiber-crossings using the mixture of Gaussian densities defined as

$$G(\mathbf{x}; \mathbf{D}, t) = \frac{1}{\sqrt{(4\pi t)^3 \det(\mathbf{D})}} \exp\left(-\frac{\mathbf{x}^T \mathbf{D}^{-1} \mathbf{x}}{4t}\right) \quad (9)$$

$$M(\mathbf{x}; D_1, \dots, D_n; a_1, \dots, a_n; t) = \sum_{i=1}^n a_i G(\mathbf{x}; D_i, t) \quad (10)$$

, where \mathbf{D} is the diffusion tensor and t is the diffusion time. We use rotations of $10^{-10} \text{diag}(17, 2, 2) \text{m}^2 \text{s}^{-1}$ for the diffusion tensor in each component. Overall, we use the following three test *pdf*:

$$\begin{aligned} p_1(\mathbf{x}) &= M_1(\mathbf{x}; A_1; 1; t), \\ p_3(\mathbf{x}) &= M_2(\mathbf{x}; A_1, A_2; \frac{1}{2}, \frac{1}{2}; t) \\ p_4(\mathbf{x}) &= M_3(\mathbf{x}; A_1, A_2, A_3; \frac{1}{3}, \frac{1}{3}, \frac{1}{3}; t). \end{aligned} \quad (11)$$

, where M_n is defined as (10).

$$\begin{aligned} A_1 &= 10^{-10} \text{diag}(17, 2, 2) \text{m}^2 \text{s}^{-1} \\ A_2 &= 10^{-10} \text{diag}(2, 17, 2) \text{m}^2 \text{s}^{-1} \\ A_3 &= 10^{-10} \text{diag}(2, 2, 17) \text{m}^2 \text{s}^{-1} \end{aligned} \quad (12)$$

B. The Phantom

We design a phantom model to simulate intersecting fibers. It consists of sheets of parallel plastic capillaries with the inner diameter of 50 μm and outer diameter of 350 μm (PTFE ultramicrobore tubing P-06417-70, Cole-Parmer Instrument, Vernon Hills, IL). The capillaries are filled with water, and sheets of two different orientations intersecting at 90° are stacked on each other in an interleaved fashion. To

secure the orientation, we wound the plastic capillaries and fasten them to a firm plastic plate notched at the corners.

C. The Comparing Method

We simulation measurement errors in synthetic data as

$$A^*(q) = |A(q) + c| \quad (13)$$

, where $c \sim N(0, \sigma^2)$, and

$$SNR \equiv \frac{A(0)}{\sigma} \quad (14)$$

A range of SNR from 4 to 32 will be applied for each technique. And the performance will be evaluated by the ratio of successfully extracting the correct number of principle direction(s), each within $\arccos(0.95)$ from the real direction(s). We define the ratio as consistency index C.

IV. RESULT

In both DTI and DTI with directional uncertainty, due to the limitation of the fitting model, they can only resolve the synthetic data p_1 . While encountering fiber crossings such as in p_3 and p_4 , they will acquire single false direction. To compare consistency index C for PAS and DSI under different SNR, an optimal parameter r for PAS has been determined.

For simulation, we choose parameters corresponding to clinical settings, that is, $|\mathbf{q}| = 2.0 \times 10^5 \text{m}^{-1}$, which distributed with 54 unique directions, together with 6 measurements of zero gradients, and $t = 0.04\text{s}$ in PAS. And in DSI, $|\mathbf{q}|$ is assigned from $1.2 \times 10^5 \text{m}^{-1}$ to $6.0 \times 10^5 \text{m}^{-1}$, determined by maximizing C under $SNR = 16$ in p_4 . The simulation result of C under different SNR for PAS and DSI is shown in Fig. 1.

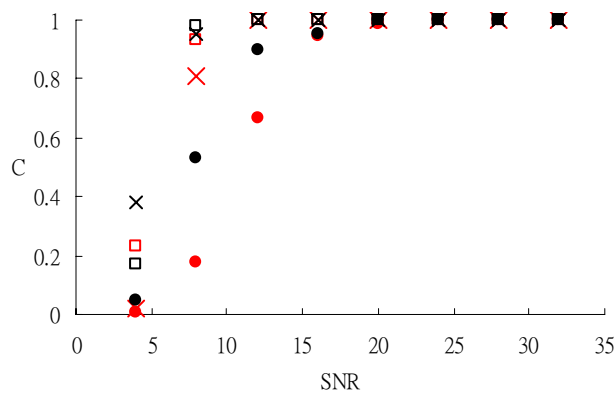


Fig.1. C under different SNR for PAS(black) and DSI(red). \square : p_1 , \times : p_3 , \bullet : p_4 . 300 trials were done for each point.

From the figure above, we may see that PAS acquires higher C under SNR from 4 to 32 except a slight difference in p_1 when SNR equals 4. The difference in p_1 may be recovered for PAS with applying more gradients. We will do more phantom studies to verify the simulation result.

V. CONCLUSION

In this paper, we state four techniques in extracting principle direction(s) from DW-MRI measurement. A comparing method is proposed, and we have done computer simulation on synthetic data to assess the performance of acquiring correct directional information from noisy measurements.

We found that both DTI and DTI with directional uncertainty cannot resolve crossing fibers while both PAS and DSI can. We also found that PAS is able to generally acquire higher consistency index C under different SNR than DSI, with on-line scanning time less than one-eighth. Since less scanning time means less motional artifact in MRI, if only directional information is concerned, PAS may have higher chance to acquire correct fiber directions in human brain during *in vivo* studies. However, while PAS requires longer post-processing time than DSI by several orders, there may be a trade-off to consider about.

REFERENCES

- [1] P. J. Basser, J. Mattiello, and D. LeBihan, "Estimation of the effective self-diffusion tensor from the NMR spin echo," *Journal of Magnetic Resonance, Series B* 103, 1994, pp. 247-254.
- [2] S. Mori, B. J. Crain, V. P. Chachko, and P. C. van Zijl, "Three-dimensional tracking of axonal projections in the brain by magnetic resonance imaging," *Ann. Neurol.*, vol. 45, no. 2, 1999, pp. 265-269.
- [3] T. E. J. Behrens, M. W. Woolrich, M. Jenkinson, H. Johansen-Berg, R.G. Nunes, S. Clare, P. M. Matthews, J. M. Brady, and S. M. Smith, "Characterization and propagation of uncertainty in diffusion-weighted MR imaging," *Magnetic Resonance in Medicine*, vol. 50, 2003, pp. 1077-1088.
- [4] T. E. J. Behrens, H. Johansen-Berg, M. W. Woolrich, S. M. Smith, C. A. M. Wheeler-Kingshott, P. A. Boulby, G. J. Barker, E. L. Sillery, K. Sheehan, O. Ciccarelli, A. J. Thompson, J. M. Brady, and P. M. Matthews, "Non-invasive mapping of connections between human thalamus and cortex using diffusion imaging," *Nature Neuroscience*, vol. 6, 2003, pp.750-757.
- [5] V. J. Wedeen, T. G. Reese, D. S. Tuch, M. R. Weigel, J. G. Dou, R. M. Weiskoff, and D. Chessler, "Mapping fiber orientation spectra in cerebral white matter with Fourier-transform diffusion MRI," *Proc. Int. Soc. Magn. Reson. Med. ISMRM, California*, p. 82.
- [6] C. P. Lin, W. Y. I. Tseng, H. C. Cheng, and J. H. Chen, "Validation of diffusion tensor magnetic resonance axonal fiber imaging with registered manganese-enhanced optic tracts," *NeuroImage*, vol. 14, 2001, pp. 1035-1047.
- [7] C. P. Lin, V. J. Wedeen, J. H. Chen, C. Yao, and W. Y. I. Tseng, "Validation of diffusion spectrum magnetic resonance imaging with manganese-enhanced rat optic tracts and ex vivo phantoms," *NeuroImage*, vol. 19, 2003, pp. 482-495.
- [8] K. M. Jansons and D. C. Alexander, "Persistent angular structure: new insights from diffusion magnetic resonance imaging data," *Inverse Problems*, vol. 19, 2003, pp. 1031-1046.
- [9] C. Pierpaoli, P. Jezzard, P. J. Basser, A. Barnett, and G. Di Chiro, "Diffusion tensor imaging of the human brain", *Radiology* 201 637-48.